NASA Technical Paper 3044

December 1990

Oxidation Characteristics of Ti-25Al-10Nb-3V-1Mo Intermetallic Alloy

Terryl A. Wallace,
Ronald K. Clark,
Sankara N. Sankaran,
and Karl E. Wiedemann

NASA

NASA Technical Paper 3044

1990

Oxidation Characteristics of Ti-25Al-10Nb-3V-1Mo Intermetallic Alloy

Terryl A. Wallace
and Ronald K. Clark
Langley Research Center
Hampton, Virginia

Sankara N. Sankaran
and Karl E. Wiedemann
Analytical Services & Materials, Inc.
Hampton, Virginia

National Aeronautics and Space Administration
Office of Management
Scientific and Technical Information Division

Abstract

Static oxidation kinetics of the super-α_2 titanium-aluminide alloy Ti-25Al-10Nb-3V-1Mo (atomic percent) were investigated in air over the temperature range of 650°C to 1000°C using thermogravimetric analysis. The oxidation kinetics were complex at all exposure temperatures and displayed up to three distinct oxidation rates. Breakaway oxidation occurred after long exposure times at high temperatures. Oxidation products were determined using X-ray diffraction techniques, electron microprobe analysis, and energy dispersive X-ray analysis. Oxide scale morphology was examined by scanning electron microscopy of the surfaces and cross sections of oxidized specimens. The oxides during the parabolic stages were compact and multilayered, consisting primarily of TiO_2 doped with Nb, a top layer of Al_2O_3, and a thin bottom layer of TiN. The transition between the second and third parabolic stage was found to be linked to the formation of a TiAl layer at the oxide-metal interface. Porosity was also formed during the third stage, causing degradation of the oxide and the beginning of breakaway oxidation.

Introduction

Titanium-aluminide intermetallic alloys, such as Ti_3Al, are candidate materials for use in hypersonic structures and advanced engines because of their high specific strength and excellent high-temperature properties. These exceptional properties result from their ordered microstructure, which is also the cause of the low ductility of intermetallic alloys at room temperature. In an effort to improve ductility, the intermetallic Ti_3Al has been alloyed with beta-stabilizing elements such as tungsten, molybdenum, niobium, tantalum, and vanadium. The alloy Ti-25Al-10Nb-3V-1Mo (atomic percent), commonly referred to as super-α_2, is one such modification of Ti_3Al being considered for aerospace applications.

The oxidation susceptibility of titanium-aluminides in hypersonic and advanced engine environments is of concern because of the reactivity of titanium alloys at high temperatures. The role of aluminum and niobium in the oxidation of titanium has been reported (refs. 1–5): aluminum reduces the solubility of oxygen in titanium, but its role on oxide formation is uncertain; and niobium decreases the oxide formation rate of titanium. Except for a few limited studies (refs. 6–11), kinetic and microstructural data on the oxidation behavior of titanium-aluminide alloys are lacking in the open literature. The existing data indicate that the kinetics for oxidation of titanium-aluminides are complex and involve two or more oxidation rates, depending on the temperature and time of exposure.

The purpose of the present study was to characterize the oxidation behavior of Ti-25Al-10Nb-3V-1Mo alloy. Samples were oxidized at temperatures over the range of 650°C to 1000°C in commercially available high-purity air (true hydrocarbon content less than 0.1 ppm) using a thermogravimetric apparatus (TGA). Selected samples were examined using X-ray diffraction (XRD), conventional light microscopy, scanning electron microscopy (SEM), microprobe X-ray analysis, energy dispersive X-ray spectroscopy (EDS), and transmission electron microscopy (TEM) to characterize the oxide composition and morphology and the microstructural changes in the metal.

Experimental Procedures

Specimens and Materials

The chemical analysis of the ingot Ti-25Al-10Nb-3V-1Mo alloy is shown in table I. The alloy in the as-received condition had been processed into a forged pancake shape (4 in. thick and 15 in. diameter) and heat treated as follows: 1121°C for 2 hr, direct transfer to 732°C salt bath for 0.5 hr, direct transfer to 816°C salt bath for 0.5 hr, and air cool.

Table I. Chemical Analysis of Ti-25Al-10Nb-3V-1Mo Alloy

Element	Atomic percent
Al	25.3
Nb	10.2
V	2.96
Mo	.979
Fe	.048
C	.091
O	.209
Ti	Remainder

TGA samples were machined to dimensions of 1 cm wide, 1.5 cm long, and 0.12 cm thick with a 0.16-cm-diameter hole through the thickness at one end for suspending the sample during the test. Surfaces of samples were ground to a uniform finish using silicon carbide paper through 2400 grit. Samples were detergent cleaned, ultrasonically cleaned in acetone and ethyl alcohol, and air dried. The dimensions of finished samples were measured to the nearest 0.001 cm and weights were recorded before and after exposure to the nearest 0.05 mg.

Oxidation Tests

Oxidation tests were conducted from 650°C to 1000°C for times up to 100 hr. The sample weight change was recorded continuously during exposure using a Cahn C2000 microbalance with an accuracy of 1 μg. Samples were suspended by quartz fibers into a vertical tubular furnace, and the temperature was monitored continuously with a type R thermocouple located just below the suspended specimen. High-purity air (true hydrocarbon content less than 0.1 ppm) was continuously pumped through the reaction chamber from the top to the bottom at a flow rate of 60 ccm. At each temperature, duplicate or triplicate tests were performed to evaluate data reproducibility.

Characterization Studies

Microstructural characterization of the alloy was done before and after oxidation using SEM, EDS, TEM, and XRD. Oxidized specimens were analyzed by XRD, SEM, and EDS to determine the oxide phases present. Selected specimens were also cross-sectioned after mounting in plastic, polished and lightly etched using Kroll's reagent (2 percent HNO_3, 1 percent HF, and 97 percent H_2O), and coated with a thin layer of gold. The cross-sectioned specimens were examined using electron microprobe, SEM, and EDS to determine the distribution and morphology of the oxide phases.

Results

Oxidation Kinetics

The oxidation of titanium alloys involves both oxide formation and dissolution of gas into the metal (ref. 12). Assuming that these processes are rate controlling, the weight will increase parabolically. This weight gain can therefore be described by the rate equation

$$m = \sqrt{k_p t}$$

where m is the weight gain per unit area of specimen surface, k_p is the parabolic rate constant, and t is time of exposure. The parabolic rate constant for a particular alloy can be calculated by plotting oxidation weight gain data in parabolic coordinates (weight as a function of square root of time), producing a line of slope $\sqrt{k_p}$. The parabolic rate constant k_p varies with temperature following the Arrhenius relation

$$k_p = k_o \exp(-Q/RT)$$

where k_o is the preexponential factor, Q is the activation energy of the rate-determining mechanism, R is the gas constant, and T is the temperature of oxidation. Using this equation, the activation energy Q is calculated by plotting $\ln(k_p)$ as a function of $1/T$, which produces a line of slope Q/R.

Examination of the weight gain kinetics for Ti-25Al-10Nb-3V-1Mo alloy using this analysis shows that there are up to three distinct stages of parabolic oxidation. All three stages were not observed for every exposure: at temperatures of 850°C and below, stages 1 and 2 were detected; at 900°C, stages 1, 2, and 3 were detected; and above 950°C, stages 2 and 3 were detected.

Figure 1 shows the weight gain history in parabolic coordinates for a specimen exposed for 100 hr at 700°C and is typical for samples exposed in the lower temperature range (650°C to 850°C) where two stages of parabolic oxidation were observed. At 700°C the first stage lasted about 7 hr, after which a second stage began at a lower oxidation rate. The periods of first-stage oxidation were shorter at higher temperatures. In fact, for exposures above 900°C the first-stage oxidation was too brief to be detected.

The weight gain history for a sample exposed for 24 hr at 1000°C is shown in figure 2. At that temperature the first stage was not observed, and only the second and third oxidation stages could be identified. The second stage lasted for 1.7 $hr^{1/2}$ (3 hr) after which there was a period of nonparabolic oxidation that lasted until 3 $hr^{1/2}$ (9 hr) when the third parabolic stage began.

Breakaway oxidation occurred after long exposure times at higher temperatures. It began at about 4.5 $hr^{1/2}$ (20 hr) for the sample exposed at 1000°C (fig. 2). Breakaway oxidation began at about 5 $hr^{1/2}$ (25 hr) for the sample exposed for 50 hr at 975°C and continued for the remainder of the test as shown in figure 3.

Table II shows TGA results for each time-temperature exposure condition, including the weight gain and the parabolic rate constant for each oxidation stage encountered. Figure 4 is an Arrhenius plot of parabolic rate constants as a function of temperature. The activation energies for super-α_2 were calculated to be 52.5 kcal/mol for the first stage, 59.5 kcal/mol for the second stage, and 23.7 kcal/mol for the third stage.

Figure 5 is an Arrhenius plot showing a comparison of the present data and similar data for Ti-24Al-10Nb (ref. 9) and Ti-25Al (ref. 11). The oxidation rates for super-α_2 are similar to those for Ti-24Al-10Nb, but both alloys have much lower rates than those of Ti-25Al.

Table II. TGA Results for Ti-25Al-10Nb-3V-1Mo

Exposure conditions		Total weight gain, mg/cm^2	Parabolic rate constant, $mg^2/cm^4/hr$		
Temp., °C	Time, hr		Stage I	Stage II	Stage III
650	100	0.101	0.000149	0.0000785	
700	100	.216	.00103	.000228	
750	100	.491	.00471	.00151	
800	24	.406	.0104	.00794	
850	24	.704	.0412	.0164	
900	24	1.08	.0807	.0357	
900	100	2.18	.0858	.0335	0.0199
950	24	*1.88		.162	
975	50	*3.42		.277	.0369
1000	24	*2.52		.426	.0437

*Oxide spalled during cooling.

Table III. Oxide Composition of Ti-25Al-10Nb-3V-1Mo From XRD Data

Exposure	Measured intensities*							
	Ti_3Al	†M_2Al	‡M_2Al	TiAl	β-Ti	TiN	TiO_2	Al_2O_3
As received	VS	S						
700°C, 100 hr	VS		S				S	
800°C, 24 hr	VS			W		S	S	W
850°C, 24 hr	S	S		W		S	S	S
900°C, 24 hr	S			S		S	VS	S
900°C, 100 hr	W			W		S	VS	S
975°C, 50 hr	S		S	S	W	VS	VS	S
1000°C, 24 hr	VS		S	S	W	VS	VS	S

*VS = very strong, S = strong, W = weak.

†M_2Al found in as-received specimen.

‡M_2Al exhibiting slightly shifted peaks and intensities.

Oxidation Products

The XRD analysis, table III, revealed that TiO_2 was the primary oxide phase formed on super-α_2 at all exposure temperatures. TiN was identified in the oxide for all specimens exposed above 700°C. The presence of Al_2O_3 varied with temperature: none was identified for samples exposed at 700°C, trace amounts were observed for samples exposed at 800°C, and significant amounts were observed for samples exposed at temperatures above 800°C. The amount of TiAl phase detected also varied with exposure temperature: trace amounts were identified in samples exposed at lower temperatures where second-stage oxidation occurs (850°C and below); significant amounts were identified in samples exposed for 24 hr at 900°C, which is just at the end of the second stage; and strong TiAl signals were identified in all samples exposed above 900°C, where third stage oxidation occurs.

SEM, EDS, and electron microprobe analysis of cross-sectioned samples were used to further characterize oxide morphologies. Samples chosen for cross-sectioning were picked to represent the various oxidation stages identified from the weight gain plots. Weight gains were too small, i.e., the oxides were too thin, during first-stage oxidation to allow analysis using this technique.

Examination of the oxides during the second parabolic stage showed multilayered, compact (void free) oxides. Figure 6 shows a cross-sectional micrograph of a specimen exposed for 24 hr at 900°C, which is at the end of the second oxidation stage. The oxide consists of three layers; the top layer is 1.8 μm thick, the middle layer is 4.7 μm thick, and the bottom layer is 1.1 μm thick. The accompanying microprobe scans, combined with the XRD results (table III), allow identification of each layer. The high nitrogen concentration in the bottom layer identifies it as TiN. The center layer is TiO_2; however, the niobium scan shows that this element is also present, decreasing in concentration from the metal-oxide interface. Since no niobium oxides were identified by XRD, it is assumed that the niobium is present in the TiO_2 as a dopant. The top layer is Al_2O_3, as shown by the high aluminum concentration. Examination of the surface of this specimen using SEM and EDS identified particles of both Al_2O_3 and TiO_2, indicating that the Al_2O_3 does not form a continuous, protective layer.

The oxides during the third parabolic stage were also found to be multilayered and compact, despite the introduction of limited porosity. Figure 7 shows the cross section of a sample exposed for 100 hr at 900°C, which is within the third oxidation stage. This sample has the same phase distribution as seen during the second stage (fig. 6): a bottom layer of TiN, a top layer of Al_2O_3, and a middle layer of TiO_2 doped with niobium. The TiN layer has not grown in thickness between 24 and 100 hr, although the Al_2O_3 and TiO_2 layers have grown from 1.8 μm to 2.8 μm and from 4.7 μm to 6.2 μm, respectively. Additionally, beneath the TiN layer a new phase has formed which has a high concentration of aluminum. This indicates that the TiAl phase identified in the XRD forms in the metal beneath the oxide-metal interface.

Oxides of samples exposed at higher temperatures, which had undergone breakaway oxidation, exhibited significantly more porosity than oxides during the second and third parabolic stages. Figure 8 shows the cross-sectional micrograph of a specimen exposed at 1000°C for 24 hr that had just started breakaway oxidation. Large amounts of porosity are visible in the oxide. The large cracks joining this porosity are assumed to have occurred during cooling or specimen preparation since the weight gain does not indicate any spalling during exposure.

New compact oxides were found to be forming underneath the oxides of specimens that had undergone long periods of breakaway oxidation. The cross-sectional micrograph of the sample exposed for 50 hr at 975°C is shown in figure 9(a). That sample experienced breakaway oxidation beginning at about 5 $hr^{1/2}$ (25 hr) and continuing for the remainder of the exposure. The TiO_2 layer had a layer of extensive porosity similar to that seen at the beginning of breakaway oxidation (fig. 8). The elemental map for aluminum (fig. 9(b)) reveals a high concentration of aluminum along the dark line visible in the oxide near the oxide-metal interface; the titanium map (fig. 9(c)) shows a depletion of titanium in this region. These indicate that a second-generation compact oxide, with the three-layer distribution of earlier compact oxides, is starting to grow beneath the original oxide.

Microstructure of Alloy

The SEM micrograph of the as-received super-α_2 (fig. 10(a)) shows an acicular, two-phase microstructure. The thin, light phase was identified by XRD and TEM as Ti_3Al. The XRD pattern of the dark phase was not found in literature; however, from XRD and TEM analysis it was found to have a structure similar to Nb_2Al. The dark phase was therefore identified as $(Ti,Nb,Mo,V)_2Al$, which will be referred to as M_2Al. The two-phase structure was retained after all exposures, even at 1000°C (fig. 10(b)).

Results from XRD analysis of selected oxidized samples are presented in table III. The XRD analysis

showed Ti_3Al was present after all exposures. The M_2Al phase was also present after all exposures but slightly modified (compared with the phase in the as-received material) after exposure at the higher temperatures (975°C and 1000°C), as revealed by different XRD extinctions and intensities. Trace amounts of β-Ti were also detected after exposure at 975°C and 1000°C.

Since the oxidation of titanium alloys proceeds by the dual processes of oxide formation and oxygen dissolution into the metal, the amount of oxygen dissolved into the alloy is an important consideration. The estimated weight gain contributions of both oxide formation and oxygen dissolution are presented in table IV. For each oxide layer, weight gain per unit area, w_o, due to oxide growth is given by

$$w_o = \rho z$$

where ρ is the density of the oxide phase and z is the thickness of this phase measured from SEM cross-sectional micrographs. Subtracting this total weight for all three oxide layers from the total weight gain yields the weight of oxygen dissolved into the metal.

Table IV. Oxide Partitioning of Oxygen in Ti-24Al-10Nb-3V-1Mo

Exposure conditions		Oxide thickness, μm	Weight gain, mg/cm^2	
Temp., °C	Time, hr		Oxide	Metal
700	100	1.0	0.17	0.04
800	24	1.6	.27	.13
900	100	10.3	1.80	.38
1000	24	11.3	1.92	.60

The compositional broadening of an X-ray diffraction peak was analyzed (ref. 13) to determine the concentration profile for oxygen in the substrate alloy for a sample exposed at 650°C for 100 hr (fig. 11). The oxygen solubility limit was estimated to be 7.5 atomic percent, and the diffusion coefficient 5.6×10^{-14} cm^2/sec was calculated. The maximum solubility was lower than the 12.5 atomic percent calculated for Ti-24Al-10Nb. The diffusion coefficients are similar; Ti-24Al-10Nb was found to have a diffusion coefficient of 4×10^{-14} cm^2/sec at 650°C. (ref. 9).

Discussion

Study of the oxidation kinetics of super-α_2 revealed complex behavior: three distinct stages of parabolic oxidation, separated by periods of non-steady-state behavior, were identified. Although similar multiple-stage oxidation behavior has been observed in other titanium-aluminide alloys, the exact mechanisms have yet to be fully identified. In the present study, the oxide morphology of representative samples were examined in some detail to better understand the operative oxidation mechanisms.

The first oxidation stage was identified only during exposure at lower temperatures and decreased in duration as the exposure temperature was increased. Because the oxides formed during first-stage oxidation were so thin, microstructural evaluation was not attempted. The activation energy calculated from the Arrhenius plot of parabolic rate constants (fig. 4) for this stage was 52.5 kcal/mol and is similar to that for the oxidation of titanium (ref. 14). This indicates that the rate of oxidation is controlled by transport across TiO_2 on the surface of the alloy.

Onset of second-stage oxidation follows first-stage oxidation after a very brief transition period. The second stage, which has a lower oxidation rate than the first, was identified at all exposure temperatures. Examination of a sample in this second stage (fig. 6) shows a compact oxide layer. The oxide consisted primarily of TiO_2 doped with niobium as identified by XRD (table II) and elemental scans. The outer surface is primarily Al_2O_3, and there is a layer of TiN at the oxide-metal interface.

The morphology observed for samples undergoing second-stage oxidation suggests a strong oxygen activity gradient across the oxide, which would result from a compact oxide. A low-oxygen activity at the oxide-metal interface is indicated by the presence of the TiN layer since the reaction to form TiN ($2TiN + O_2 = 2TiO + N_2$) requires a very low partial pressure of oxygen to proceed, $P_{O_2}/P_{N_2} = 5 \times 10^{-16}$ at 982°C (ref. 15). The presence of Al_2O_3 only at the surface also confirms the steep activity gradient. Since the solubility of Al_2O_3 in TiO_2 (rutile) is a strong function of oxygen activity (increasing as the activity of oxygen decreases (ref. 16)), Al_2O_3 would be soluble within the oxide, where the oxygen activity is low. The Al_2O_3 would exist as a distinct phase only at the surface, where there is a high oxygen activity.

The layer of Al_2O_3, however, was not shown to be protective. XRD, SEM, and EDS analysis of the oxide surface of a sample exposed for 24 hr at 900°C showed the presence of Al_2O_3 and TiO_2 particles, indicating that the Al_2O_3 layer was discontinuous and allowed titanium to diffuse to the surface. Examining the oxidation kinetics data also indicated that the Al_2O_3 was not protective. The activation energy was calculated to be 59.5 kcal/mol for the second oxidation stage, which is similar to that for the oxidation of titanium alloys. This indicates that transport across the TiO_2 layer is rate controlling, and that Al_2O_3 has

little effect on the oxidation rate. These facts imply that the presence of Al_2O_3 at the surface has little or no effect on oxidation rates.

The super-α_2 was shown to have an oxygen solubility of 7.5 atomic percent, which is lower than that of titanium alloys. This is attributed in part to the presence of aluminum, which has been shown to reduce the maximum oxygen solubility of titanium alloys (ref. 17). Beta-stabilizers (niobium, molybdenum, and vanadium) have been shown to reduce the oxidation rate of titanium alloys by reducing the alloy oxygen solubility (ref. 17). In addition the presence of niobium in the oxide, as shown in figure 6, has been attributed with slowing the diffusion of oxygen through the oxide by reducing the concentration of oxygen ion vacancies (ref. 9).

Despite the lower oxygen solubility, oxygen dissolution into the metal must still be considered. As little as 1.2 atomic percent oxygen has been shown to embrittle titanium (ref. 18), and this level has been exceeded for a depth of 4 μm after 100 hr at 650°C (fig. 11). This could have serious consequences on the mechanical properties when super-α_2 is used as a thin sheet.

The second-stage oxidation kinetics obey the classical parabolic law. The kinetics are determined by both transport across a compact oxide surface and oxygen dissolution into the metal substrate. Although Al_2O_3 does form on the surface, it does not create a protective surface and in fact has little impact on the oxidation kinetics.

At higher temperatures the oxide layer becomes unstable, and the oxidation kinetics depart from steady-state parabolic behavior. After some transition period a third parabolic stage was observed, but this lasted only a short period at 975°C and 1000°C; thereafter breakaway oxidation was observed (figs. 2 and 3). The XRD revealed that the primary difference between the second and third stages was the presence of TiAl. Only trace amounts of TiAl were found in samples within the second stage, but a strong XRD signal from XRD was identified at the end of the second stage (900°C, 24 hr). The TiAl was still observed by XRD during the third stage (900°C, 100 hr) and also clearly visible in the cross-sectional micrographs (see fig. 7). Smaller amounts of TiAl were observed in specimens that experienced breakaway oxidation (1000°C, 24 hr and 975°C, 50 hr).

Based on this analysis, the TiAl phase plays a major role in altering the parabolic processes governing the second-stage oxidation. Aluminum is rejected back into the metal as oxidation proceeds, creating a layer of high aluminum concentration at the metal-oxide interface and the eventual nucleation of TiAl particles. The presence of the TiAl alters the diffusion across the oxide and disturbs the parabolic growth of the oxide. There is a period of non-parabolic growth as this TiAl grows, and once this layer completely covers the oxide-metal interface a new rate of diffusion is established causing a new parabolic oxidation rate. These kinetics dominate the third parabolic oxidation stage.

SEM examination of cross-sectioned third-stage specimens also revealed the presence of limited porosity, in contrast to the compact oxides formed during second-stage oxidation. Layered porosity found in Ti alloys has been attributed to successive spallation events caused by stresses between the growing oxide and the oxygen-saturated metal substrate (ref. 19). The super-α_2 alloy has a lower oxygen solubility than titanium alloys and therefore does not undergo similar spallation. However, the formation of the TiAl does introduce a complicated stress situation that may be linked to the formation of porosity.

According to Mrowec (ref. 20), porosity interrupts the diffusion both of metal ions to the surface and of oxygen ions to the oxide-metal interface. The oxygen activity begins to increase next to the pore, with a corresponding increase in the oxygen pressure in the pore. The oxide begins to dissociate surrounding the pore, and fills the pores with a new porous oxide product. If this process continues, it can degrade the protectiveness of the oxide as more of the oxide is converted into this nonprotective form.

Specimens exposed at 975°C and 1000°C exhibited breakaway oxidation, and their oxides had extensive porosity (figs. 8 and 9). It would appear that porosity continues to form during the third oxidation stage until the process of dissociation begins to render the oxide unprotective and breakaway oxidation begins. At 975°C after 20 hr of breakaway oxidation, the process of dissociation had proceeded to the point that a second-generation oxide was able to form at the oxide-metal interface.

Concluding Remarks

Super-α_2 titanium-aluminide alloy Ti-25Al-10Nb-3V-1Mo is a modification of the stoichiometric alloy Ti_3Al that was developed to improve room-temperature ductility for aerospace applications. Additions of vanadium and molybdenum do not significantly alter the oxidation characteristics of the alloy compared with Ti-24Al-10Nb alloy. Noteworthy features of the oxidation behavior of super-α_2 are as follows:

1. The overall oxidation rate is much lower than for stoichiometric Ti_3Al alloy and about the same as for Ti-24Al-10Nb alloy.

2. The oxidation kinetics are marked by at least three distinct parabolic stages with successively lower oxidation rates. The occurrence of the stages depends on the exposure time and temperature.
3. The oxidation products are TiO_2 doped with Nb, Al_2O_3, and TiN, but Al_2O_3 does not contribute to the protection of the alloy.
4. Oxidation during the parabolic stages is controlled by the presence of compact oxides. The transition between the second stage and the third stage is linked to the formation of a TiAl layer at the oxide-metal interface.
5. Breakaway oxidation occurs after long times at high temperatures. The oxides during this stage exhibit large amounts of porosity that reduce their protectiveness.
6. Oxygen dissolution in the alloy must be considered during the oxidation of super-α_2. The solubility of oxygen in the alloy is lower than that of Ti-24Al-10Nb, but their diffusivities are the same.

NASA Langley Research Center
Hampton, VA 23665-5225
September 28, 1990

References

1. Chaze, A. M.; and Coddet, C.: Influence of Alloying Elements on the Dissolution of Oxygen in the Metallic Phase During the Oxidation of Titanium Alloys. *J. Mat. Sci.*, vol. 22, Apr. 1987, pp. 1206–1214.
2. Streiff, R.; and Poize, S.: Oxidation of Aluminide Coatings on Unalloyed Titanium. *High Temperature Corrosion*, R. A. Rapp, ed., National Association of Corrosion Engineers, 1983, pp. 591–597.
3. Perkins, R. A.; Chiang, K. T.; and Meier, G. H.: Formation of Alumina on Ti-Al Alloys. *Scr. Metall.*, vol. 21, no. 11, Nov. 1987, pp. 1505–1510.
4. Hauffe, Karl: *Oxidation of Metals*. Plenum Press, 1965.
5. Chen, Y. S.; and Rosa, C. J.: High-Temperature Oxidation of Ti-4.32 wt.% Nb Alloy. *Oxid. Metals*, vol. 14, no. 2, Apr. 1980, pp. 147–165.
6. Zelenkov, I. A.; and Osokin, E. N.: Oxidation Resistance of the Compound Ti 3Al and Its Alloys at Temperatures of 700 and 800 C. *Poroshkovaia Metall.*, vol. 14, no. 10, Oct. 1975, pp. 72–75.
7. Zelenkov, I. A.; and Martynchuk, E. N.: Heat Resistance of Alloys of the Compound TiAl With Niobium at 800 and 1000 C. *Metallofizika*, no. 42, 1972, 63–66.
8. Khobaib, M.; and Vahldiek, F. W.: High Temperature Oxidation Behavior of Ti_3Al Alloys. *Space Age Metals Technology—2nd International SAMPE Metals and Metals Processing Conference, Volume 2*, F. H. Froes and Ray A. Cull, eds., Soc. for the Advancement of Material and Process Engineering, 1988, 262–270.
9. Sankaran, Sankara N.; Clark, Ronald K.; Unnam, Jalaiah; and Wiedemann, Karl E.: *Oxidation Characteristics of Ti-14Al-21Nb Alloy*. NASA TP-3012, 1990.
10. Meier, G. H.; Appalonia, D.; Perkins, R. A.; and Chiang, K. T.: Oxidation of Ti-Base Alloys. *Oxidation of High-Temperature Intermetallics*, Toni Grobstein and Joseph Doychak, eds., Minerals, Metals & Materials Soc., 1988, pp. 185–193.
11. Welsch, G.; and Kahveci, A. I.: Oxidation Behavior of Titanium Aluminide Alloys. *Oxidation of High-Temperature Intermetallics*, Toni Grobstein and Joseph Doychak, eds., Minerals, Metals & Materials Soc., 1988, 207–218.
12. Kofstad, P.; Anderson, P. B.; and Krudtaa, O. J.: Oxidation of Titanium in the Temperature Range 800–1200°C. *J. Less-Common Metals*, vol. 3, no. 2, Apr. 1961, pp. 89–97.
13. Wiedemann, K. E.; and Unnam, J.: A Method of Rapidly Obtaining Concentration-Depth Profiles From X-Ray Diffraction. *J. Appl. Phys.*, vol. 58, no. 3, Aug. 1, 1985, pp. 1095–1101.
14. Chaze, A. M.; Coddet, C.; and Béranger, G.: Influence de L'Aluminium sur la Tenue à L'Oxydation du Titane Entre 550 et 750°C. *J. Less-Common Metals*, vol. 83, 1982, pp. 49–70.
15. Wiedemann, K. E.; Sankaran, S. N.; Clark, R. K.; and Wallace, T. A.: Static and Dynamic Oxidation of Ti-14Al-21Nb. *Oxidation of High-Temperature Intermetallics*, Toni Grobstein and Joseph Doychak, eds., Minerals, Metals & Materials Soc., 1988, pp. 195–206.
16. Kofstad, Per: *Nonstoichiometry, Diffusion, and Electrical Conductivity in Binary Metal Oxides*. John Wiley & Sons, Inc., c.1972.
17. Perkins, R. A.; Chiang, K. T.; Meier, G. H.; and Miller, R.: Formation of Alumina on Niobium and Titanium Alloys. *Oxidation of High-Temperature Intermetallics*, Toni Grobstein and Joseph Doychak, eds., Minerals, Metals & Materials Soc., 1988, pp. 157–169.
18. Gupta, D.; and Weinig, S.: The Dislocation-Oxygen Interaction in Alpha Titanium and Its Effect on the Ductile-to-Brittle Transition. *Trans. Metall. Soc.* AIME, vol. 215, no. 1, 1959, pp. 209–216.
19. Bertrand, G.; Jarraya, K.; and Chaix, J. M.: Morphology of Oxide Scales Formed on Titanium. *Oxid. Metals*, vol. 21, nos. 1 & 2, 1983, pp. 1–19.
20. Mrowec, S.: On the Mechanism of High Temperature Oxidation of Metals and Alloys. *Corros. Sci.*, vol. 7, no. 2, 1967, pp. 563–578.

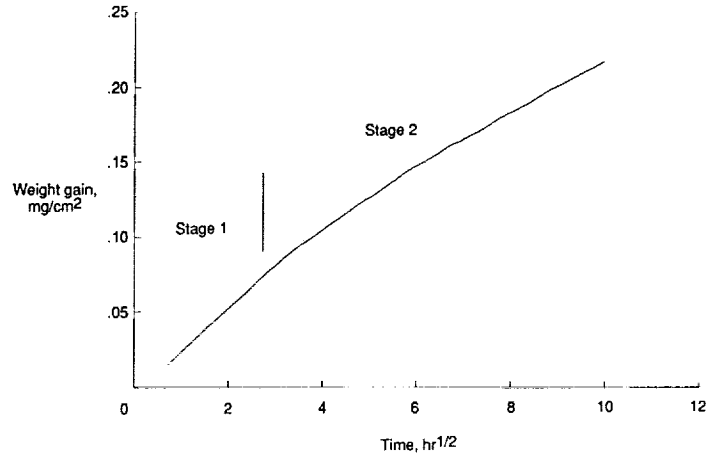

Figure 1. TGA results in parabolic coordinates for 100 hr exposure at 700°C for Ti-25Al-10Nb-3V-1Mo.

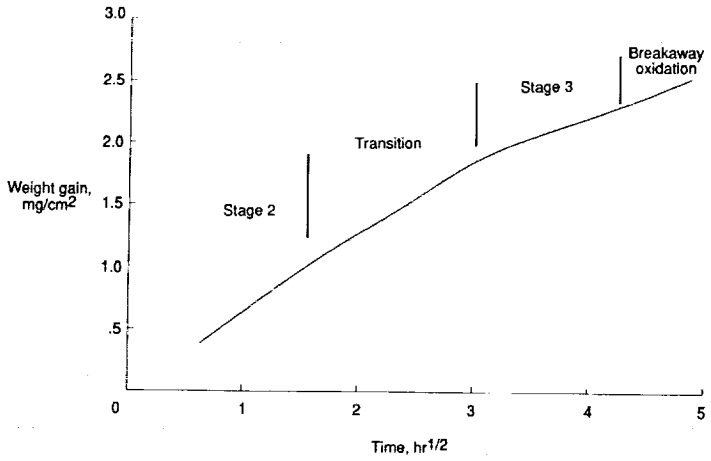

Figure 2. TGA results in parabolic coordinates for 24 hr exposure at 1000°C for Ti-25Al-10Nb-3V-1Mo.

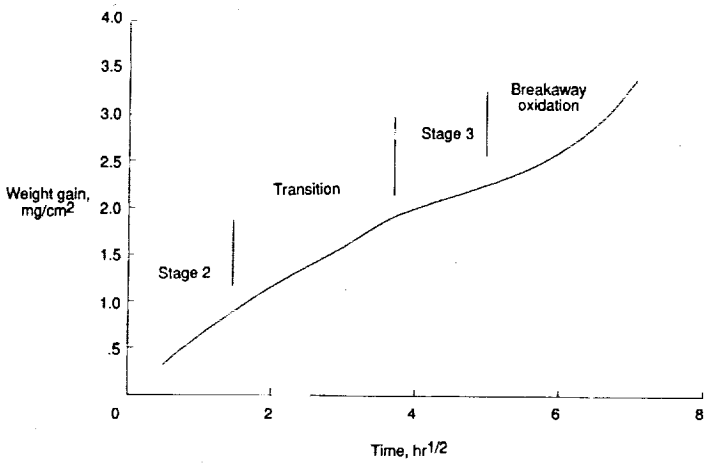

Figure 3. TGA results in parabolic coordinates for 50 hr exposure at 975°C for Ti-25Al-10Nb-3V-1Mo.

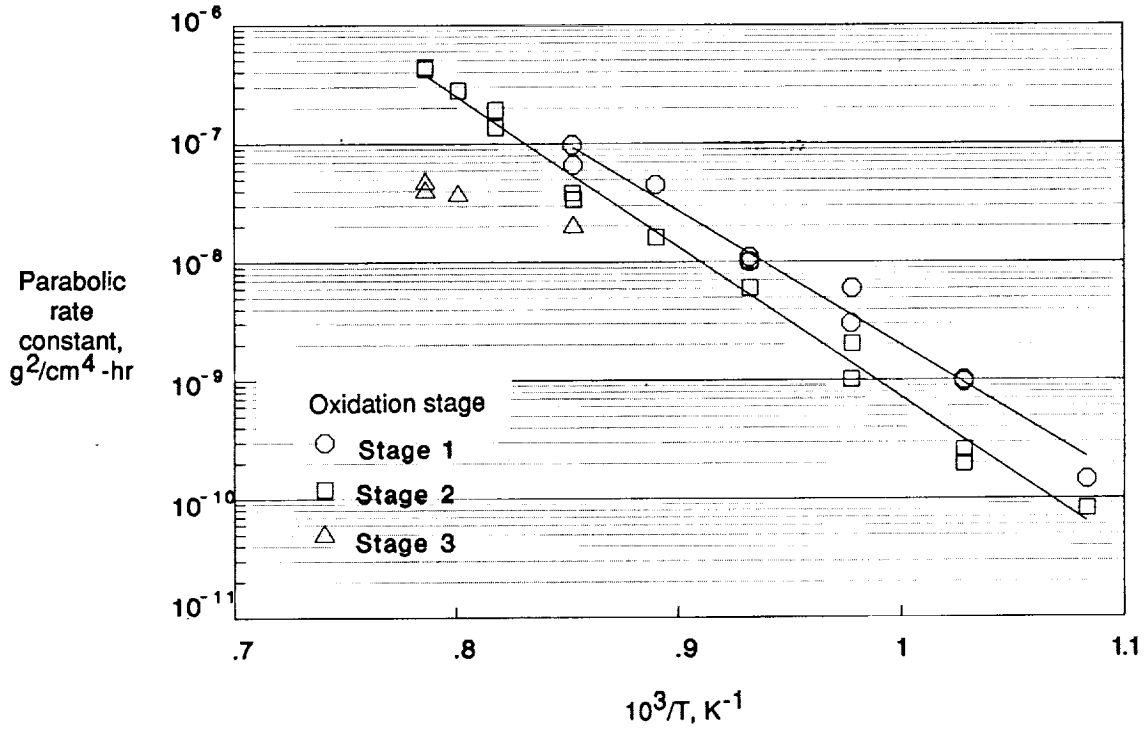

Figure 4. Arrhenius plot of oxidation rates for Ti-25Al-10Nb-3V-1Mo showing oxidation stages.

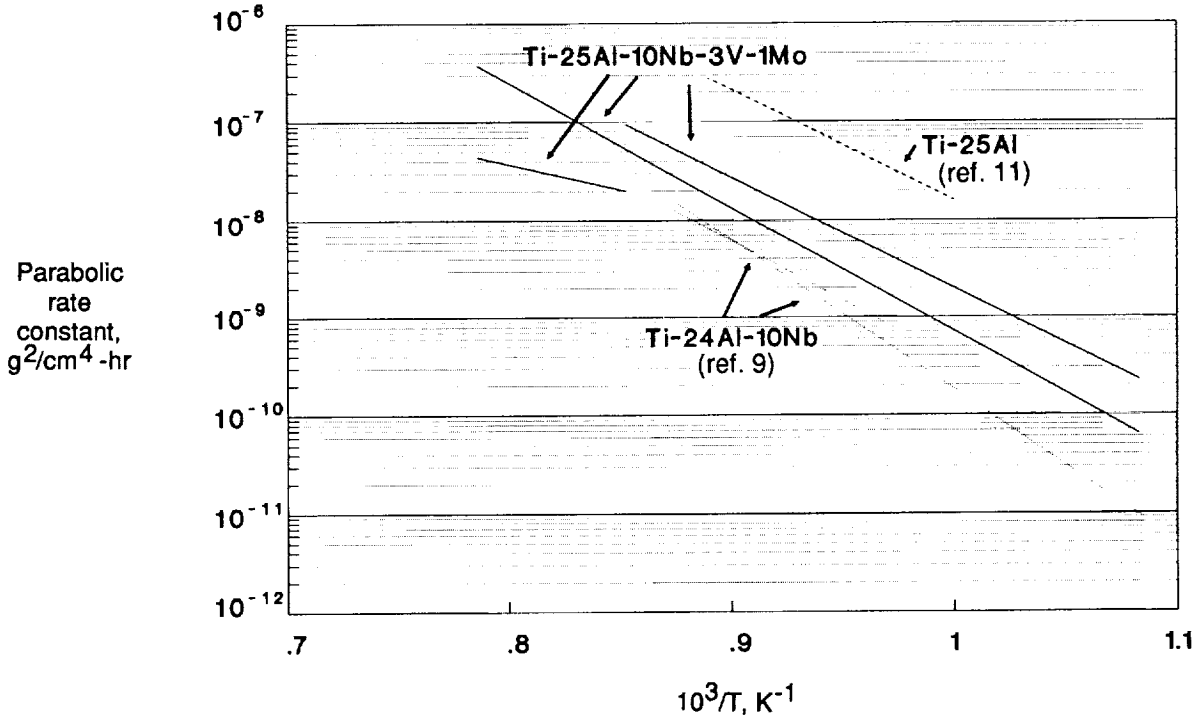

Figure 5. Arrhenius plot of oxidation rates for titanium-aluminide alloys.

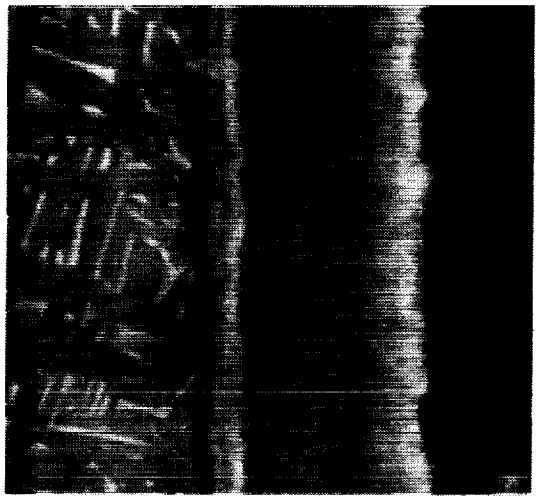

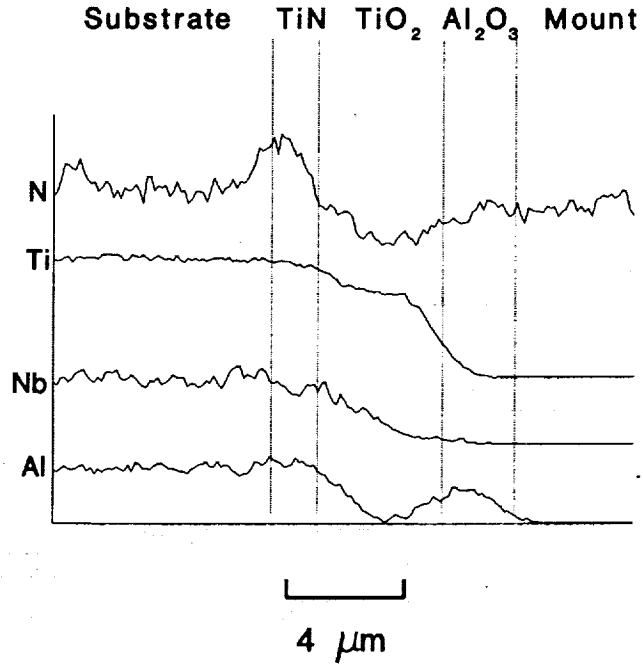

Figure 6. SEM micrograph and microprobe elemental scans for Ti-25Al-10Nb-3V-1Mo exposed at 900°C for 24 hr.

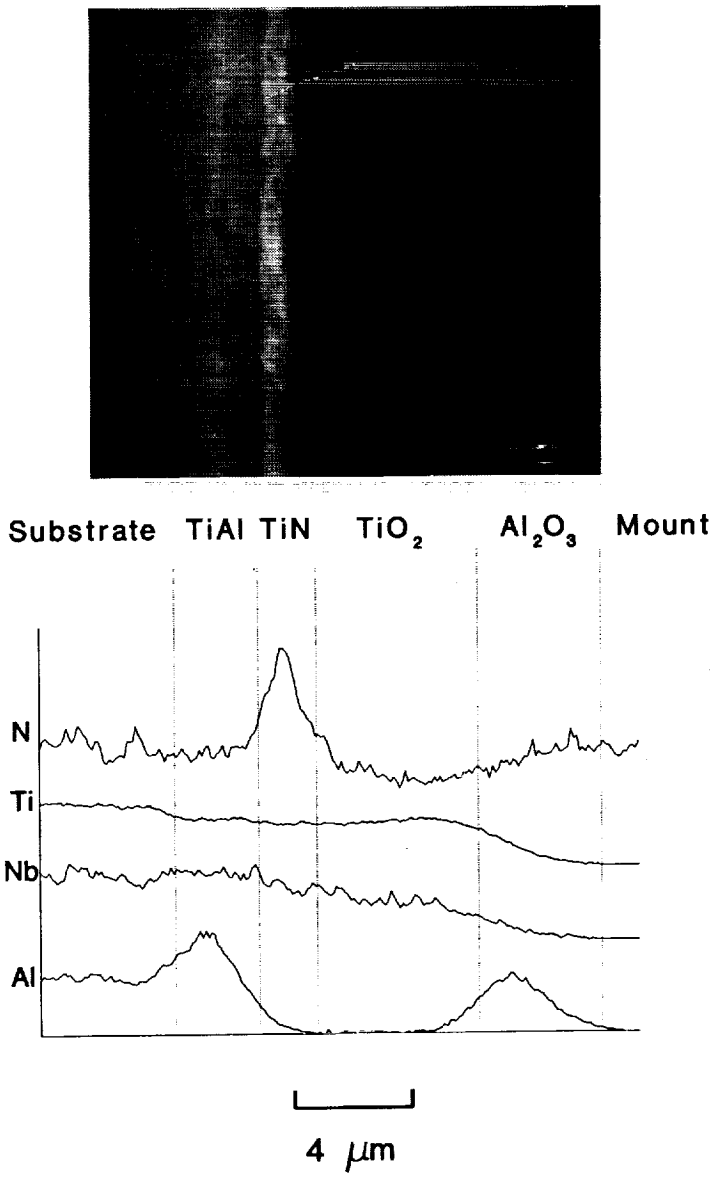

Figure 7. SEM micrograph and microprobe elemental scans for Ti-25Al-10Nb-3V-1Mo exposed at 900°C for 100 hr.

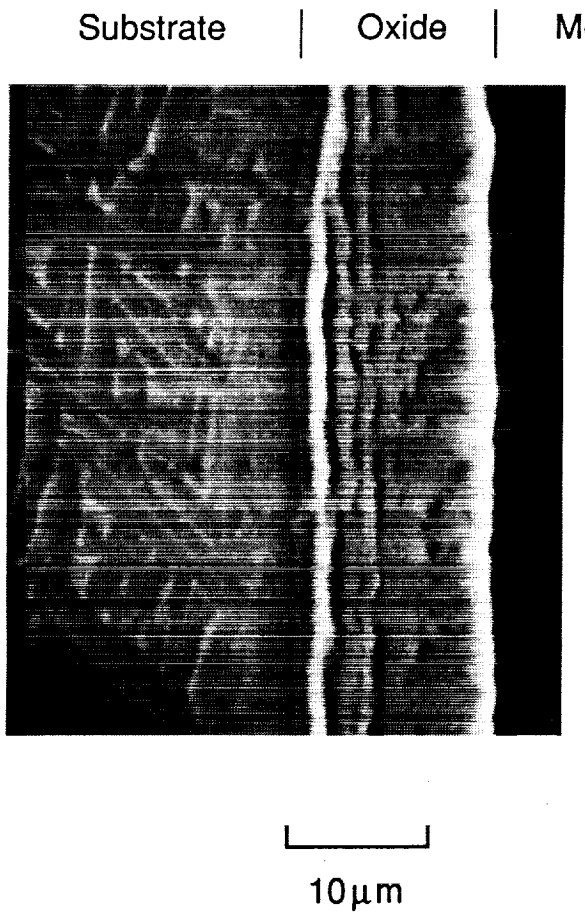

Figure 8. SEM micrograph of Ti-25Al-10Nb-3V-1Mo exposed at 1000°C for 24 hr.

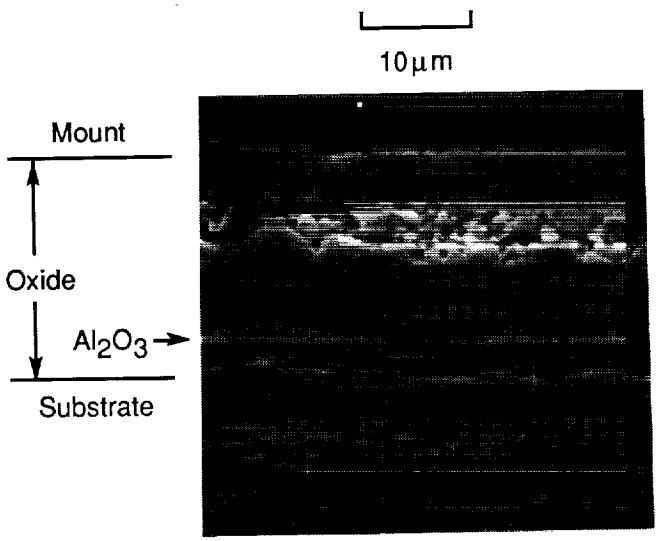

(a) SEM micrograph.

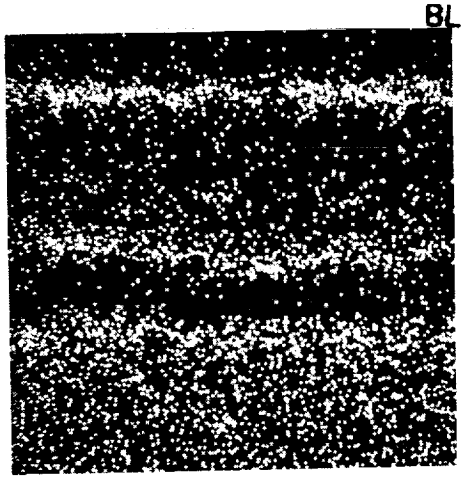

(b) Elemental map of aluminum.

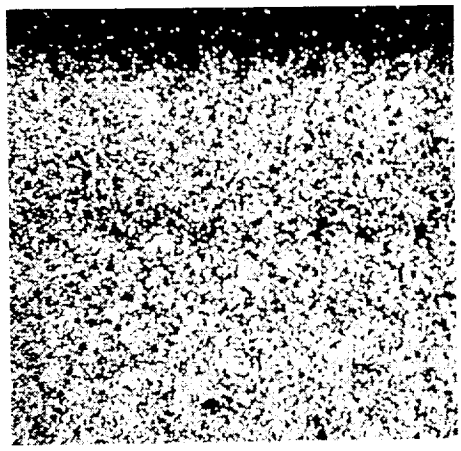

(c) Elemental map of titanium.

Figure 9. Ti-25Al-10Nb-3V-1Mo exposed at 975°C for 50 hr.

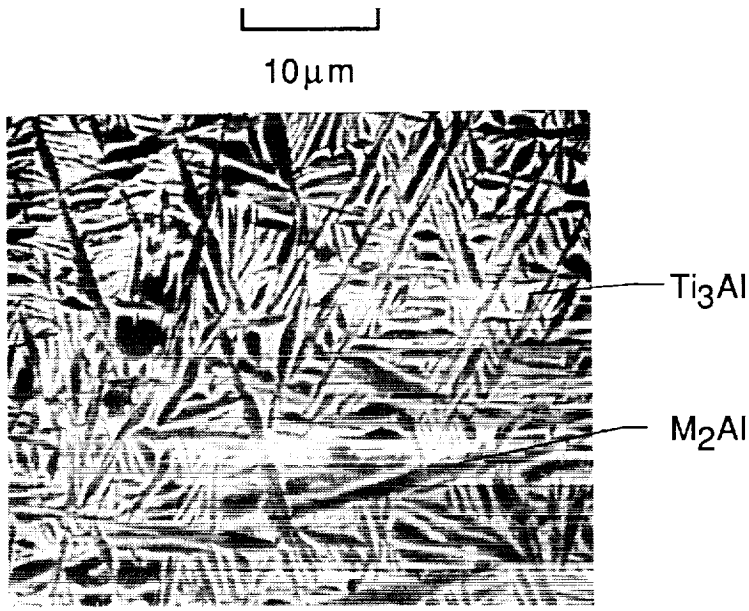

(a) As received.

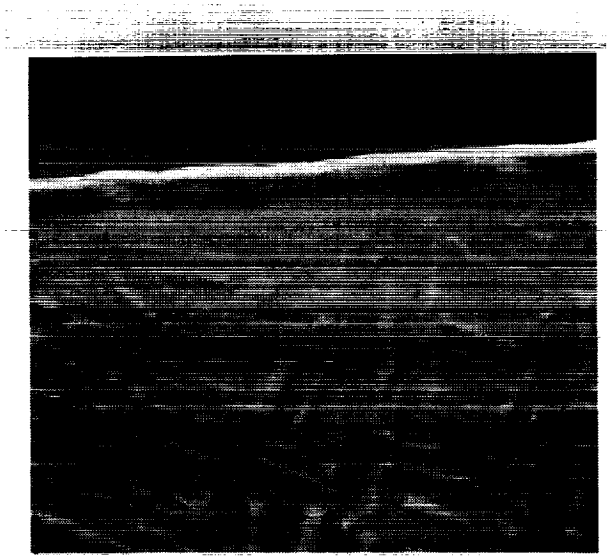

(b) After 24 hr exposure at 1000°C.

Figure 10. SEM micrographs of Ti-25Al-10Nb-3V-1Mo microstructure.

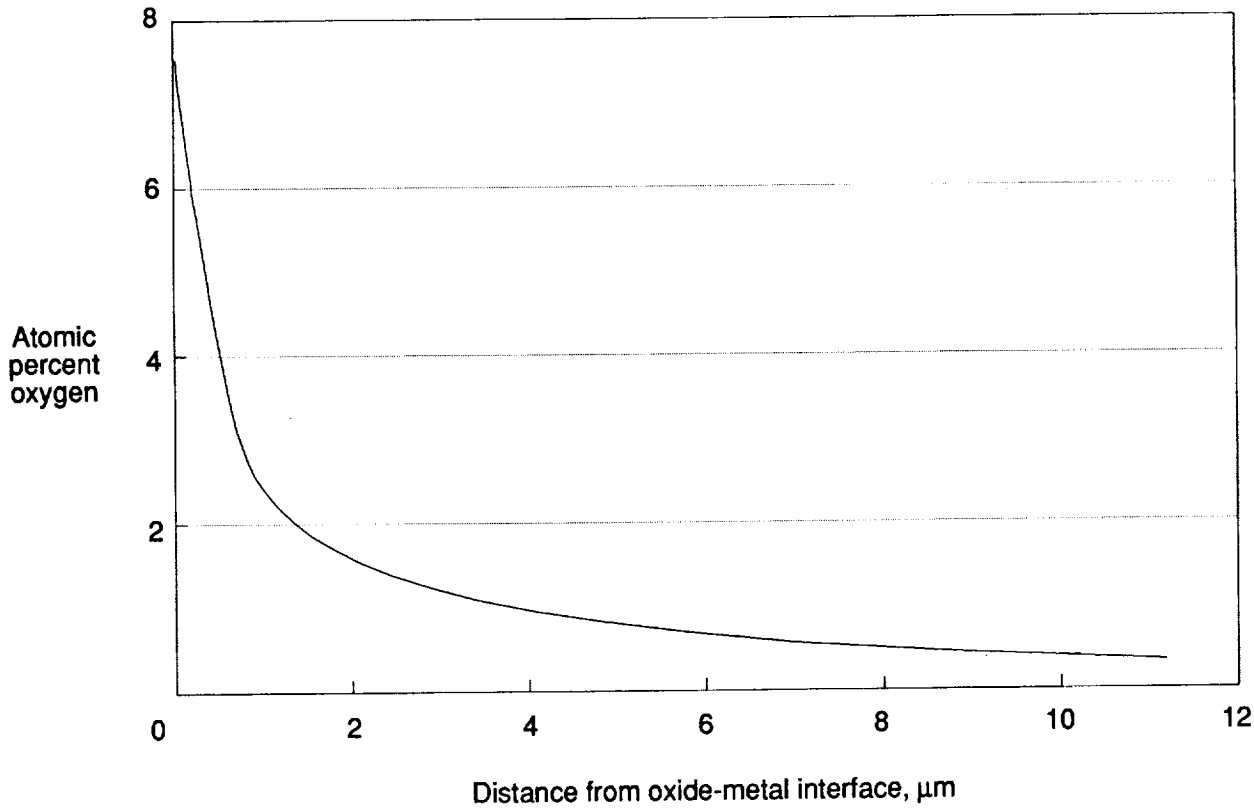

Figure 11. Composition-depth profile of oxygen in Ti-25Al-10Nb-3V-1Mo determined from compositional broadening of an X-ray diffraction peak. Specimen exposed for 100 hr at 650°C.

NASA
National Aeronautics and Space Administration

Report Documentation Page

1. Report No.	2. Government Accession No.	3. Recipient's Catalog No.
NASA TP-3044		

4. Title and Subtitle	5. Report Date
Oxidation Characteristics of Ti-25Al-10Nb-3V-1Mo Intermetallic Alloy	December 1990
	6. Performing Organization Code
7. Author(s)	8. Performing Organization Report No.
Terryl A. Wallace, Ronald K. Clark, Sankara N. Sankaran, and Karl E. Wiedemann	L-16808
9. Performing Organization Name and Address	10. Work Unit No.
NASA Langley Research Center Hampton, VA 23665-5225	506-43-71-01
	11. Contract or Grant No.
12. Sponsoring Agency Name and Address	13. Type of Report and Period Covered
National Aeronautics and Space Administration Washington, DC 20546-0001	Technical Paper
	14. Sponsoring Agency Code

15. Supplementary Notes

Terryl A. Wallace and Ronald K. Clark: Langley Research Center, Hampton, Virginia.
Sankara N. Sankaran and Karl E. Wiedemann: Analytical Services & Materials, Inc., Hampton, Virginia.

16. Abstract

Static oxidation kinetics of the super-α_2 titanium-aluminide alloy Ti-25Al-10Nb-3V-1Mo (atomic percent) were investigated in air over the temperature range of 650°C to 1000°C using thermogravimetric analysis. The oxidation kinetics were complex at all exposure temperatures and displayed up to three distinct oxidation rates. Breakaway oxidation occurred after long exposure times at high temperatures. Oxidation products were determined using X-ray diffraction techniques, electron microprobe analysis, and energy dispersive X-ray analysis. Oxide scale morphology was examined by scanning electron microscopy of the surfaces and cross sections of oxidized specimens. The oxides during the parabolic stages were compact and multilayered, consisting primarily of TiO_2 doped with Nb, a top layer of Al_2O_3, and a thin bottom layer of TiN. The transition between the second and third parabolic stages was found to be linked to the formation of a TiAl layer at the oxide-metal interface. Porosity was also formed during the third stage, causing degradation of the oxide and the beginning of breakaway oxidation.

17. Key Words (Suggested by Authors(s))	18. Distribution Statement
Oxidation Titanium aluminides Intermetallic alloys	Unclassified—Unlimited Subject Category 26

19. Security Classif. (of this report)	20. Security Classif. (of this page)	21. No. of Pages	22. Price
Unclassified	Unclassified	16	A03

For sale by the National Technical Information Service, Springfield, Virginia 22161-2171